

Effect of Solution Temperature on Electrodeposition Behavior of Zn-Ni Alloy from Alkaline Zincate Solution

Bae, Sung Hwa
Graduate School of Engineering, Kyushu University

Oue, Satoshi
Faculty of Engineering, Kyushu University

Taninouchi, Yu-ki
Faculty of Engineering, Kyushu University

Son, Injoon
Department of Materials Science and Metallurgy, Kyungpook National University

他

<https://hdl.handle.net/2324/7172646>

出版情報 : ISIJ International. 62 (7), pp.1522-1531, 2022-07-15. 日本鉄鋼協会
バージョン :
権利関係 : © 2022 The Iron and Steel Institute of Japan.



Effect of Solution Temperature on Electrodeposition Behavior of Zn–Ni Alloy from Alkaline Zincate Solution

Sung Hwa BAE,¹⁾ Satoshi OUE,²⁾ Yu-ki TANINOUCHI,²⁾ Injoon SON³⁾ and Hiroaki NAKANO^{2)*}

1) Graduate School of Engineering, Kyushu University, 744, Motooka, Nishi-ku, Fukuoka-shi, 819-0395 Japan.

2) Faculty of Engineering, Kyushu University, 744, Motooka, Nishi-ku, Fukuoka-shi, 819-0395 Japan.

3) Department of Materials Science and Metallurgy, Kyungpook National University, 80 Daehak-ro, Sangyeok-dong, Buk-gu, Daegu, 41566 Korea.

(Received on February 21, 2022; accepted on March 25, 2022; originally published in *Tetsu-to-Hagané*, Vol. 108, 2022, No. 2, pp. 120–130)

Zn–Ni alloys were electrodeposited on a Cu electrode at $10\text{--}500\text{ A}\cdot\text{m}^{-2}$ and $5 \times 10^4\text{ C}\cdot\text{m}^{-2}$ in an unagitated zincate solution at 293, 313, and 333 K. The effect of solution temperature on the electrodeposition behavior of Zn–Ni alloys from alkaline zincate solutions was investigated. The transition current density at which the deposition behavior shifted from a normal to an anomalous co-deposition was almost identical at 293 and 313 K but increased at 333 K, due to enhanced H_2 evolution and Ni deposition at 333 K. The current efficiency for alloy deposition increased with solution temperature in both the normal ($10\text{--}50\text{ A}\cdot\text{m}^{-2}$) and anomalous ($500\text{ A}\cdot\text{m}^{-2}$) co-deposition regions. In the normal co-deposition region, Ni deposition and H_2 evolution mainly occurred, and the current efficiency increased with solution temperature due to the stronger promotional effect of increase in solution temperature on Ni deposition. In the anomalous co-deposition region at $500\text{ A}\cdot\text{m}^{-2}$, Zn deposition and H_2 evolution mainly occurred, and Zn deposition appeared to proceed based on a mixed rate-determining process comprising the charge transfer and diffusion of Zn ions. The current efficiency increased with solution temperature due to the acceleration of the Zn ions diffusion. The Ni content in the deposited films increased with the solution temperature at all the current densities, since Ni deposition was accelerated to a greater degree than Zn deposition by increasing the solution temperature in the region where the charge transfer process was rate-limiting. The γ -phase of the deposited films also increased with increasing solution temperature.

KEY WORDS: zincate; zinc–nickel alloy; electrodeposition; solution temperature; anomalous co-deposition; polarization curve; current density; transition current; current efficiency; charge transfer.

1. Introduction

Zn electrodeposition has long been used to prevent the corrosion of steel sheets, while Zn alloy electrodeposition has been used to further improve the corrosion resistance of the deposited films.^{1–8)} Among Zn alloy depositions, Zn–Ni alloy coatings are often applied on the various industrial fields such as automobile parts, and building materials, owing to their superior thermal stability and corrosion resistance. Zn–Ni alloys are usually deposited in a sulfate or chloride solution; however, considering the throwing power on small parts, the use of a zincate solution is preferable. Zn–Ni alloy depositions from sulfate and chloride solutions have been studied a lot so far, and are known to lead to anomalous co-deposition behavior, in which the electrochemically less-noble Zn is preferentially deposited

over noble Ni in the practical current density range.^{9–15)} Although the effect of current density,^{16–19)} total concentration of metal ions,²⁰⁾ agitation of solution,¹⁹⁾ concentration of Ni complexing agent¹⁹⁾ and solution composition^{17,19–21)} and the effect of current density^{18,20)} on the current efficiency for alloy deposition were reported in Zn–Ni alloy deposition from the zincate solutions, few studies on the deposition mechanism²²⁾ have been reported compared with those on sulfate and chloride.

Solution temperature is known to affect the overpotential, throwing power, metal salt solubility, and solution conductivity.²³⁾ Increasing the solution temperature increases the diffusion coefficient of ions in solution and solubility of the metal salt, as well as conductivity of the solution, which consequently increases the diffusion-limiting current density. In contrast, when the solution temperature is decreased, the crystal grain of the deposits becomes finer, and the throwing power is improved, based on the increases

* Corresponding author: E-mail: nakano@zaiko.kyushu-u.ac.jp



in the deposition overpotential. Thus, solution temperature is a highly important factor in electrodeposition. However, the effect of solution temperature on the deposition behavior of the Zn–Ni alloys from zincate solutions has rarely been reported.¹⁹⁾ In the present study, this topic is discussed, based on the partial polarization curves of Zn and Ni depositions and H₂ evolution.

2. Experiment

Table 1 shows the zincate solution composition and electrolysis conditions for the Zn–Ni alloy deposition. The electrolytic solutions were prepared by dissolving reagent-grade ZnO (0.15 mol·dm⁻³), NiSO₄·6H₂O (0.016 mol·dm⁻³), N(CH₂CH₂OH)₃ (0.34 mol·dm⁻³), and NaOH (2.5 mol·dm⁻³) in distilled and deionized water at room temperature. In some experiments, the deposition behavior was investigated using a solution containing only Ni or Zn, eliminating the ZnO (0.15 mol·dm⁻³) or NiSO₄·6H₂O (0.016 mol·dm⁻³) from the solution noted above. Electrodeposition was carried out by the constant-current electrolysis method, without stirring, at current densities of 10–500 A·m⁻², an amount of charge of 5 × 10⁴ C·m⁻², and solution temperatures of 293, 313, and 333 K. The amount of charge of 5 × 10⁴ C·m⁻² corresponded to a film thickness of 2.37 μm, assuming the deposition of pure Zn at a current efficiency of 100%. A Cu plate (1 × 2 cm) was used as the cathode and a Pt plate (1 × 2 cm) as the anode, respectively. However, when preparing samples for scanning electron microscopy (SEM) observation and X-ray diffraction (XRD) analysis, an Fe plate (1 × 2 cm) was used as the cathode. The obtained electrodeposits were dissolved in HNO₃, and Zn and Ni were quantified by inductively coupled plasma-optical emission spectroscopy (ICP-OES) to determine the composition of the deposited alloy and the current efficiency of the Zn and Ni depositions. The current efficiency of the H₂ evolution was calculated by subtracting the current efficiencies (%) of Zn and Ni from 100, and the partial current densities of Zn and Ni depositions and H₂ evolution were calculated by multiplying the total current density by the current efficiency (%) / 100. The partial current densities for Zn and Ni depositions and H₂ evolution were calculated by multiplying the total current density by their respective current efficiencies (%) / 100. The current efficiencies for Ni and Zn depositions from the solution with only Ni or Zn were calculated using the same method as for alloy deposition. An Ag/AgCl electrode (saturated KCl, 0.199 V vs. NHE, 298 K) was used as a reference electrode to measure the polarization curve, but the potential was converted to a standard hydrogen electrode and displayed. The surface morphology of the deposited

films was observed by SEM, and the phase identification was carried out by XRD (Cu-Kα, tube voltage = 40 kV, tube current = 15 mA).

3. Results

3.1. Effect of Solution Temperature on the Deposition Behavior of Zn–Ni Alloys

Figure 1 shows the total polarization curve of the Zn–Ni alloy deposition and the partial polarization curves of Zn and Ni depositions and H₂ evolution. The equilibrium potential, $E_{\text{Zn}}^{\text{eq}}$, of the Zn deposition ($\text{ZnO}_2^{2-} + 2\text{H}_2\text{O} + 2\text{e}^- \rightarrow \text{Zn} + 4\text{OH}^-$) was –1.27 V, assuming pure Zn deposition.²⁴⁾ The total polarization curve (Fig. 1(a)) rose in the nobler potential region compared with the equilibrium potential of Zn (–1.27 V), regardless of the solution temperature. Furthermore, it significantly shifted to the less-noble potential region when the current density exceeded 50–100 A·m⁻², and rose again when the potential reached the equilibrium potential of Zn. At all the potential region nobler and less noble than the equilibrium potential of Zn, comparing the potential at the constant total current density, the potential shifted to noble direction with increasing solution temperature. At solution temperatures of 293 and 313 K, the current density range in which the cathode potential shifted significantly from the region nobler than the equilibrium potential of Zn to the equilibrium potential was 50–100 A·m⁻². At 333 K, it was as high as 100–200 A·m⁻².

The partial polarization curve of the Zn deposition (Fig. 1(b)) rose in the nobler potential region than the equilibrium potential of Zn, as with the total polarization curve, regardless of the solution temperature. It then shifted to the less-noble potential region, before sharply rising when it reached a potential less-noble region than the equilibrium potential of Zn (–1.27 V). In both potential regions, the partial polarization curve of the Zn deposition shifted to the noble direction as the solution temperature increased. For the Zn–Ni alloy deposition, the current density for Zn deposition was only slightly detected, even at approximately –0.9 V, a value nobler than its equilibrium potential. Comparing the current density at a constant potential of –0.9 V, the current density of Zn deposition increased with increasing solution temperature.

The equilibrium potential, $E_{\text{Ni}}^{\text{eq}}$ for Ni deposition ($\text{Ni}(\text{TEA})_2^{2+} + 2\text{e}^- \rightarrow \text{Ni} + 2\text{TEA}$) was –0.41 V. This was calculated by assuming that pure Ni had been deposited, based on the complex stabilization constant $K = 10^{4.74, 25)}$ which was formed by the coordination of two triethanolamine molecules toward Ni²⁺ ions. Similar to the total polarization curve, the partial polarization curve of the Ni deposition (Fig. 1(c)) also rose in the potentially nobler region compared with the equilibrium potential of Zn, regardless of the solution temperature. It then shifted to the less-noble potential region and rose again at potentials less noble than the equilibrium potential of Zn (–1.27 V). In both potential regions, the partial polarization curve of the Ni deposition shifted to nobler potential direction as the solution temperature increased.

The H₂ evolution in the Zn–Ni alloy solution (Fig. 1(d)) rose in the region nobler than the equilibrium potential of Zn, decreased once (despite the shift in the potential to the

Table 1. Solution compositions and electrolysis conditions.

ZnO	(mol·dm ⁻³) 0.15	Current density (A·m ⁻²)	10–500
NiSO ₄ ·6H ₂ O	(mol·dm ⁻³) 0.016	Temperature (K)	293, 313, 333
N(CH ₂ CH ₂ OH) ₃	(mol·dm ⁻³) 0.34	Amount of charge (C·m ⁻²)	5 × 10 ⁴
NaOH	(mol·dm ⁻³) 2.5	Cathode	Cu (1 × 2 cm ²)
Quiescent bath		Anode	Pt (1 × 2 cm ²)

negative direction), and increased again in the region that was less noble than the equilibrium potential of Zn. The partial polarization curve of the H_2 evolution did not differ significantly at solution temperatures of 293 and 313 K. In contrast, at 333 K, it was clearly depolarized (*i.e.*, the electrode potential shifted to a nobler value when comparing the electrode potential at a constant-current density), and the current density at which the potential sharply shifted to the less-noble direction was higher than those measured at 293 and 313 K.

Figure 2 shows the correlation between the current efficiency and current density for Zn–Ni, Zn, and Ni depositions and H_2 evolution during Zn–Ni alloy deposition at different temperatures. The current efficiency of Zn–Ni alloy deposition is the sum of the current efficiencies of Zn and Ni depositions. As shown in Fig. 2(a), the current efficiency of the alloy deposition at a solution temperature of 293 K was low, ranging from 14% to 26% in the low-current density range of $10\text{--}50\text{ A}\cdot\text{m}^{-2}$. However, it sharply increased when the current density exceeded $50\text{ A}\cdot\text{m}^{-2}$ and reached a maximum at $100\text{ A}\cdot\text{m}^{-2}$. It then decreased as the current density further increased. A similar trend was observed at 313 K, although the current efficiency was slightly higher in the low and high-current density ranges of $10\text{--}50\text{ A}\cdot\text{m}^{-2}$ and $500\text{ A}\cdot\text{m}^{-2}$, respectively. Contrastingly, at a solution temperature of 333 K, the current efficiency was low, ranging from 18% to 52% in the low-current density range of $10\text{--}100\text{ A}\cdot\text{m}^{-2}$, although it significantly increased when the current density exceeded $100\text{ A}\cdot\text{m}^{-2}$ and reached a

maximum at $250\text{ A}\cdot\text{m}^{-2}$. The current efficiency rarely decreased, even when the current density was increased to $500\text{ A}\cdot\text{m}^{-2}$. At solution temperatures of 293 and 313 K, the current efficiency of Zn deposition during alloy deposition (Fig. 2(b)) was very low in the low-current density range of $10\text{--}50\text{ A}\cdot\text{m}^{-2}$, and it was also very low in the range of $10\text{--}100\text{ A}\cdot\text{m}^{-2}$ at 333 K. However, it increased sharply when the current density exceeded 50 and $100\text{ A}\cdot\text{m}^{-2}$, respectively. The current efficiency of Ni deposition during alloy deposition (Fig. 2(c)) also decreased with increasing current density, regardless of the solution temperature. Furthermore, the current efficiency of Ni deposition was higher at higher solution temperature. In the low-current density range of $10\text{--}50\text{ A}\cdot\text{m}^{-2}$ at solution temperatures of 293 and 313 K, and in the range of $10\text{--}100\text{ A}\cdot\text{m}^{-2}$ at 333 K, H_2 evolution had the highest current efficiency (Fig. 2(d)), followed by Ni deposition. However, in the high-current density range above $50\text{--}100\text{ A}\cdot\text{m}^{-2}$, the current efficiency of Zn deposition was the highest. Thus, the current efficiency of Zn–Ni alloy deposition reflected the current efficiency of Ni deposition in the low-current density region and that of Zn deposition in the high-current density region.

The current efficiency of Zn deposition (Fig. 2(b)) was also compared with the total polarization curve shown in Fig. 1(a). The range of $10\text{--}50\text{ A}\cdot\text{m}^{-2}$ was nobler than the equilibrium potential of Zn at solution temperatures of 293 and 313 K, and the current efficiency of Zn deposition was thus considered as being low. When the current density exceeded $50\text{ A}\cdot\text{m}^{-2}$, the potential shifted to the less-noble

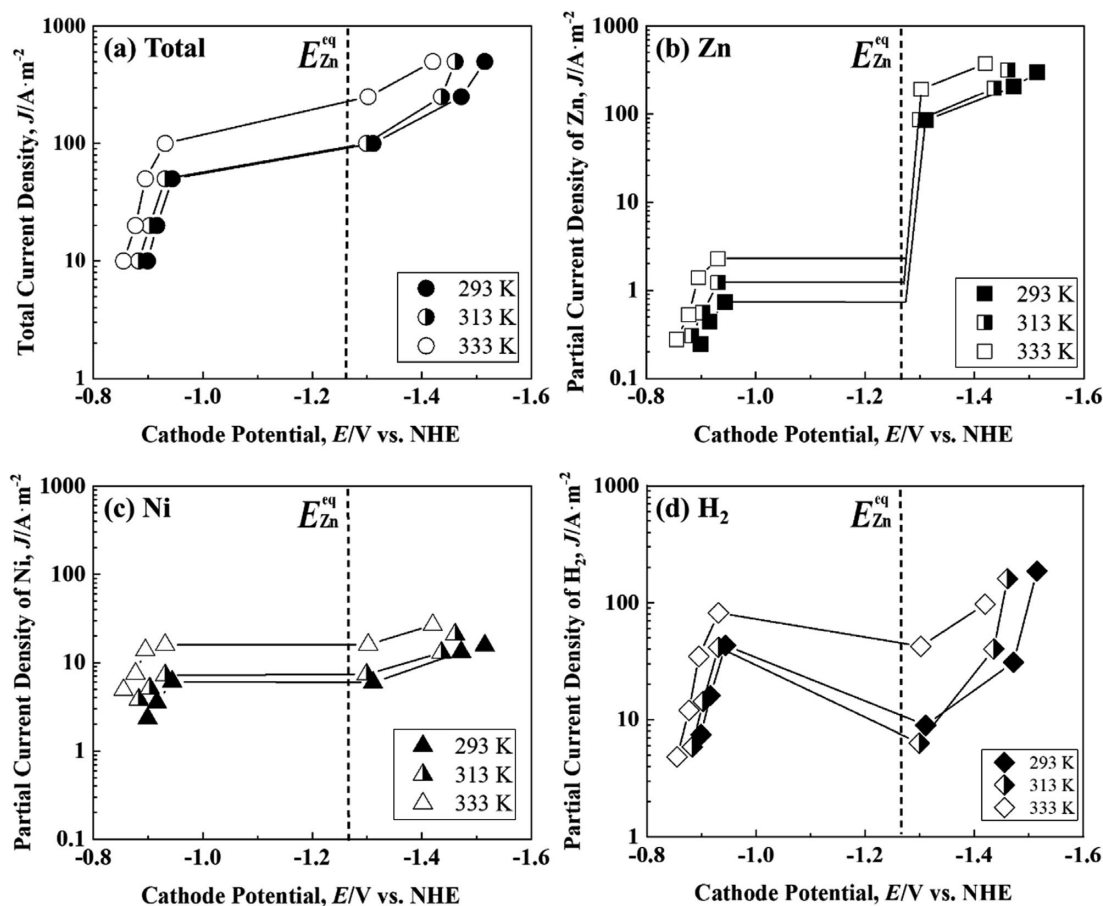


Fig. 1. Polarization curves for Zn–Ni alloy deposition at 293, 313 and 333 K [(a) Total polarization curves, partial polarization curves of (b) Zn, (c) Ni and (d) H_2].

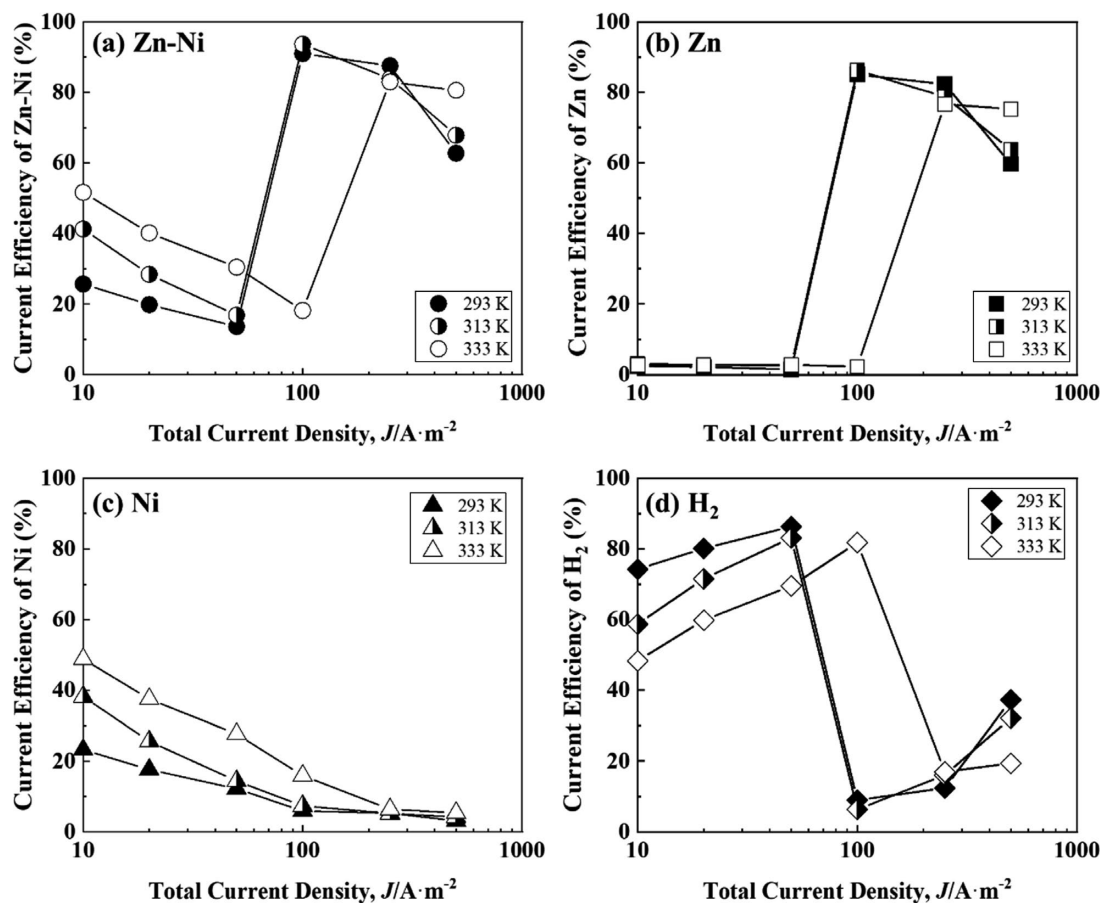


Fig. 2. Current efficiencies for Zn–Ni alloy deposition at 293, 313 and 333 K [(a) Zn–Ni, (b) Zn, (c) Ni and (d) H₂].

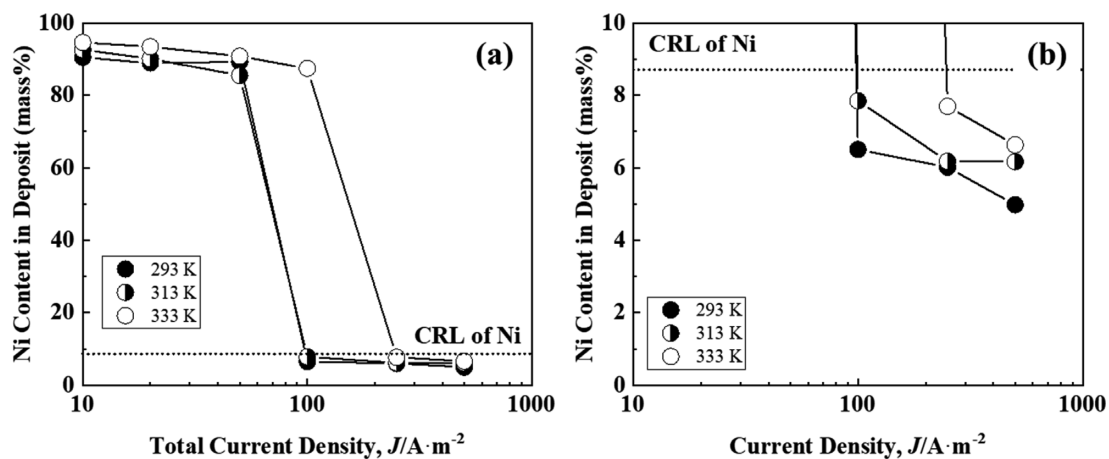


Fig. 3. Ni contents in the Zn–Ni alloys deposited at various current densities from different temperatures. (b) Magnified view of the area of 0–10 mass% of the Ni content.

region compared with the equilibrium potential of Zn (Fig. 1(a)), therefore, the current efficiency of Zn seems to increase sharply. At a solution temperature of 333 K, the potential was nobler than the equilibrium potential of Zn in the range of 10–100 $A \cdot m^{-2}$. However, when the current density exceeded 100 $A \cdot m^{-2}$, the potential shifted to a potential range less noble than the equilibrium potential of Zn (Fig. 1(a)), resulting in a sharp increase in the current efficiency of Zn. Thus, the current densities at which the current efficiency sharply changed, at all measured temperatures, corresponded to those at which the cathode potential changed from the potential region nobler than the equilib-

rium potential of Zn to that of the equilibrium potential of Zn in the total polarization curve. The decrease in the current efficiency at 500 $A \cdot m^{-2}$ at solution temperatures of 293 and 313 K appeared to have been caused by the fact that the Zn deposition approached the diffusion limit of the Zn ions.

Figure 3 shows the effect of the current density on the Ni content of the Zn–Ni alloy films. The broken line (the compositional reference line [CRL] of Ni) represents the Ni content in the deposits predicted from the concentration ratio of Ni ions against the total metal ions in the solution. When the Ni content in the deposited films exceeded the CRL, a normal co-deposition occurred, with electrochemically

noble Ni being preferentially deposited over Zn. In contrast, when the Ni content in the deposited films was lower than the CRL, an anomalous co-deposition occurred, with base Zn being deposited preferentially over Ni. As shown in Fig. 3, the Ni content in the deposited films altered significantly in the range of 50–100 $\text{A}\cdot\text{m}^{-2}$ at solution temperatures of 293 and 313 K. At current densities below 50 $\text{A}\cdot\text{m}^{-2}$, the Ni content in the deposited films was approximately 90 mass% above the CRL, indicating the normal co-deposition, while at current densities above 100 $\text{A}\cdot\text{m}^{-2}$, the Ni content in the deposited films was below the CRL, indicating the anomalous co-deposition. In contrast, at 333 K, the Ni content in the deposited films was significantly altered in the region from 100 to 250 $\text{A}\cdot\text{m}^{-2}$. Below 100 $\text{A}\cdot\text{m}^{-2}$, the Ni content in the deposited films was above the CRL, indicating the normal co-deposition. Above 250 $\text{A}\cdot\text{m}^{-2}$, the Ni content in the deposited films was below the CRL, indicating the anomalous co-deposition. The current density at which the deposition behavior shifts from normal to anomalous is called the transition current density.^{26–28)} At all the solution temperatures, the transition current density corresponded to the current density at which the potential of the total polarization curve shown in Fig. 1(a) abruptly shifted to the less-noble potential region, or to the current density at which the current efficiency significantly changed (Fig. 2(b)). As described above, the transition current density at 293 K was almost identical to that at 313 K, although it was higher at 333 K. The Ni content in the films increased with increasing solution temperature in the low-current density range, where the normal co-deposition was observed. The Ni content in the deposited films also increased slightly with increasing solution temperature in the current density range

above 250 $\text{A}\cdot\text{m}^{-2}$ at which the anomalous co-deposition occurred (Fig. 3(b)).

3.2. Effect of Solution Temperature on the Microstructure of Deposited Films

Figure 4 shows the X-ray diffraction patterns of the films obtained at various current densities from the solutions at different temperatures. Three main peaks were observed in the films obtained at 10 $\text{A}\cdot\text{m}^{-2}$ (Figs. 4(a)–4(c)). The diffraction angles of the substrate Fe and α -Ni phases (solid solution of Zn in the Ni) overlapped at 44.7° , making it difficult to identify the α -phase. Therefore, we investigated the XRD pattern of the substrate Fe only and confirmed that the peak intensity at a diffraction angle of 44.7° was smaller than that at 65.0° . However, it was larger than that at 65.0° for the deposited film obtained at 10 $\text{A}\cdot\text{m}^{-2}$, regardless of the solution temperature; it was thus concluded that the α -phase existed in all the deposited films. Weak peaks indicating the presence of the α -phase were also detected at diffraction angles other than 44.7° in the deposited films obtained at 333 K. The deposition at 10 $\text{A}\cdot\text{m}^{-2}$ exhibited the normal co-deposition, regardless of the solution temperature, and the Ni content in the deposited films was above 90 mass%. As a result, only the α -phase was thought to be detected. No peaks related to Zn, obtained by underpotential co-deposition, were detected. In the deposited films obtained at 100 $\text{A}\cdot\text{m}^{-2}$, the η -phase (solid solution of Ni in the Zn) and γ -phase (intermetallic compound $\text{Ni}_2\text{Zn}_{11}$), were detected at solution temperatures of 293 and 313 K (Figs. 4(d) and 4(e)), whereas only peaks of the α -phase and Fe were detected at 333 K (Fig. 4(f)). At 100 $\text{A}\cdot\text{m}^{-2}$, the deposition behavior differed significantly, based on the solution

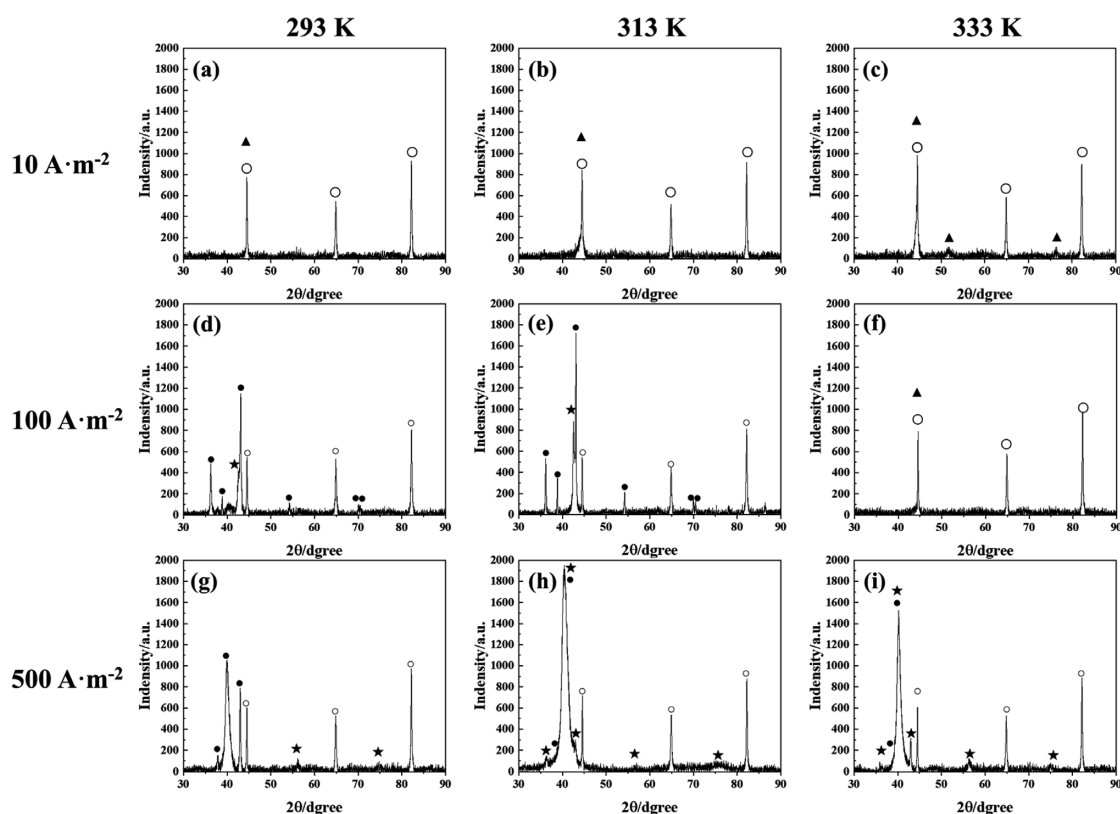


Fig. 4. X-ray diffraction patterns of the Zn–Ni alloy films deposited at various current densities from different temperatures (▲ Ni[α] PDF # 87-0712, ○ Fe PDF # 65-4899, ● Zn[η] PDF # 87-0713, and ★ $\text{Ni}_2\text{Zn}_{11}$ [γ] PDF # 65-5310).

temperature. In particular, the depositions at 293 and 313 K exhibited the anomalous co-deposition, resulting in a high Zn content (approximately 93 mass%) in the films, while the deposition at 333 K exhibited the normal co-deposition, resulting in a high Ni content (approximately 87.4 mass%; Fig. 3). The XRD patterns of the deposited films obtained at $100 \text{ A}\cdot\text{m}^{-2}$ reflected this same deposition behavior. In contrast, the η - and γ -phases were detected in the deposited films obtained at $500 \text{ A}\cdot\text{m}^{-2}$ (Figs. 4(g)–4(i)), and the formation of the γ -phase was dominant at higher solution temperatures. Since the Ni content in the deposited films increased with increasing solution temperature (Fig. 3(b)), the formation of the γ -phase seems to become easy with increasing temperature. At $100 \text{ A}\cdot\text{m}^{-2}$, the main peak of the γ -phase was higher at 313 K than at 293 K, indicating that the γ -phase had increased with temperature. These results indicated that the γ -phase increased with increasing solution temperature in the case of the anomalous co-deposition of deposited films with a high Zn content.

Figure 5 shows the SEM images of the deposited films obtained from the solutions at different temperatures and current densities. The films deposited at $10 \text{ A}\cdot\text{m}^{-2}$ were smooth at 293 K (Fig. 5(a)) but became slightly coarse at higher solution temperatures (Figs. 5(b) and 5(c)). The films obtained at $100 \text{ A}\cdot\text{m}^{-2}$ comprised the α -phase and had an Ni content of greater than 90 mass% at all the solution temperatures, while the grain size was thought to be increased as the solution temperature increased, due to a decrease in the overpotential for deposition. In the films deposited at $500 \text{ A}\cdot\text{m}^{-2}$, the agglomerations consisting of fine crystals were observed at 293 and 313 K (Figs. 5(d) and 5(e)), while at 333 K, the morphology was similar

to that of the deposited films obtained at $10 \text{ A}\cdot\text{m}^{-2}$ (Fig. 5(f)). As noted above, for the deposition at $100 \text{ A}\cdot\text{m}^{-2}$, an anomalous co-deposition was observed at 293 and 313 K, and the deposited films with approximately 7 mass% of Ni content in deposits comprised η and γ -phases, while a normal co-deposition was observed at 333 K, and the deposited films with 87.4 mass% of Ni content in deposits comprised an α -phase. The surface morphology of the films obtained at $100 \text{ A}\cdot\text{m}^{-2}$ seems to reflect the phase structure noted above. In contrast, that of the films obtained at $500 \text{ A}\cdot\text{m}^{-2}$ where an anomalous co-deposition was observed at all the temperatures, exhibited the plate-like crystal characteristics of the η -phase at a solution temperature of 293 K (Fig. 5(g)). However, this plate-like structure disappeared with increasing solution temperatures (Fig. 5(i)), and a smooth surface was observed. The films deposited at $500 \text{ A}\cdot\text{m}^{-2}$ comprised η and γ -phases, and the γ -phase became dominant with increasing solution temperature, as a result, the surface morphology seems to change.

4. Discussion

The effect of solution temperature on the deposition behavior of the Zn–Ni alloys from alkaline zincate solutions was investigated. The transition current density at which the deposition behavior shifted from the normal to anomalous, the current efficiency of the alloy deposition, and the composition of the deposited films changed depending on the solution temperature. The reasons for these effects are discussed as follows.

The partial polarization curve of Ni deposition in the alloy deposition (Fig. 1(c)) is first explained. This partial

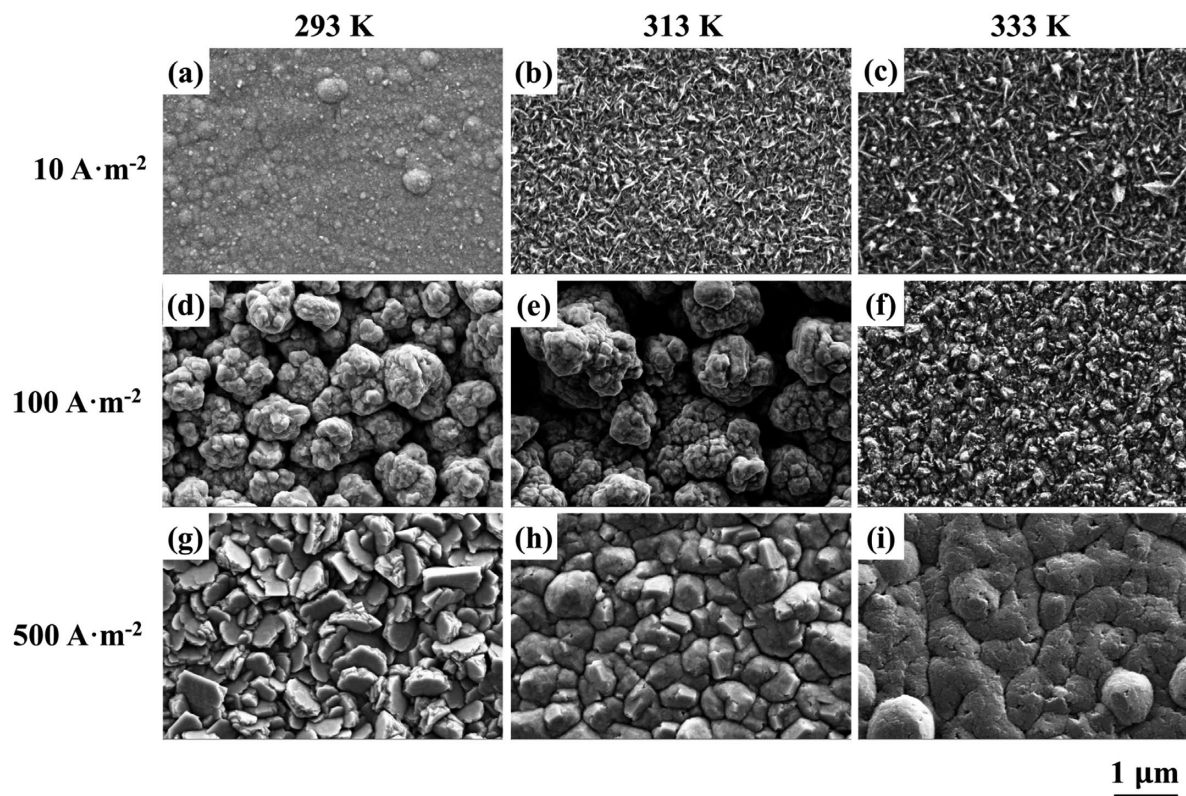


Fig. 5. SEM images of the surface of the Zn–Ni alloys deposited at various current densities from different temperatures.

polarization curve rose at approximately -0.9 V, regardless of the solution temperature, which was a nobler value than the equilibrium potential of Zn, and then sharply shifted to a less noble potential region (Fig. 1(c)). The partial current density at which the cathode potential changed sharply to a less noble potential region was similar to the diffusion-limiting current density of the Ni deposition. However, if this current density was assumed as the diffusion-limiting current density of Ni, the Ni content of the deposited films would be above the CRL in the entire current density range,^{29–31)} which would contradict the results of the present study. In fact, it has been reported that in the normal type deposition, the deposition of the noble metal becomes the diffusion-limiting current density, and the content of the noble metal in the films will be above the CRL in all the current density range.^{29–31)} In the present study, the partial current density of Ni deposition at which the cathode potential changed sharply to a less noble potential region shown in Fig. 1(c) was not the diffusion-limiting current density because the anomalous co-deposition was observed in the high-current density region.

It was reported that the transition current density in Zn–Ni alloy deposition from a sulfate solution corresponded to the current density that generated the overpotential for the H_2 evolution η_H^{inh} ; this is represented by Eq. (1) as follows:^{32–34)}

$$E_H^{eq} - \eta_H^0 - \eta_H^{inh} = E_{Zn}^{eq} \dots\dots\dots (1)$$

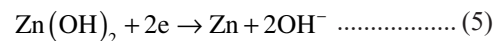
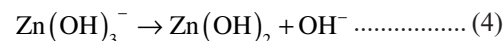
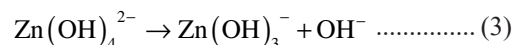
Here, E_H^{eq} and E_{Zn}^{eq} denote the equilibrium potentials for H_2 evolution and Zn deposition, respectively; η_H^0 is the minimum overpotential for H_2 evolution, and η_H^{inh} is the overpotential for H_2 evolution in the presence of its inhibitor. In the case of Zn deposition from an acidic solution, the reaction intermediate $Zn(OH)_2$ will be formed by hydrolysis of the Zn^{2+} ions ($Zn^{2+} + 2H_2O \rightarrow Zn(OH)_2 + 2H^+$), caused by the increase in pH due to H_2 evolution reaction ($2H^+ + 2e^- \rightarrow H_2$) at the cathode layer. This $Zn(OH)_2$ appears to create the overpotential for H_2 evolution, *i.e.*, η_H^{inh} .^{32–34)} In Zn–Ni alloy deposition from a sulfate solution, Ni deposition is suppressed by $Zn(OH)_2$ and becomes almost zero in the normal co-deposition region, resulting in H_2 evolution only.²⁶⁾ Therefore, to complete Eq. (1), the transition current density is defined as the H_2 evolution current density that is required to generate the overpotential, *i.e.*, η_H^{inh} .^{32–34)} However, in Zn–Ni alloy deposition from zincate solutions, Zn and Ni are deposited in the region of the normal co-deposition at potentials nobler than the equilibrium potential of Zn (Figs. 1(b), 1(c)), and the potential of Ni deposition shifts significantly to the equilibrium potential of Zn at the transition current density. Therefore, the transition current density in the zincate solution is considered to be the sum of the current densities of the H_2 evolution and Zn and Ni depositions required to satisfy both Eqs. (1) and (2).

$$E_{Ni}^{eq} - \eta_{Ni}^0 - \eta_{Ni}^{inh} = E_{Zn}^{eq} \dots\dots\dots (2)$$

Here, E_{Ni}^{eq} denotes the equilibrium potential for Ni deposition, η_{Ni}^0 is the minimum overpotential for Ni deposition, and η_{Ni}^{inh} is the overpotential for Ni deposition in the presence of its inhibitor.

It was reported that the inhibitor of H_2 evolution and Ni deposition in Zn–Ni alloy deposition from acidic solutions

was $Zn(OH)_2$, which was formed by the hydrolysis of Zn^{2+} ions.³⁴⁾ However, no hydrolysis reaction of the Zn^{2+} ions occurs in zincate solutions. Generally, Zn deposition from a zincate solution has been reported to proceed by the multistep reactions shown in Eqs. (3)–(5),^{35–37)}



In Zn–Ni alloy deposition from a zincate solution, the $Zn(OH)_2$ formed during the multistep reactions is thought to act as an inhibitor for the H_2 evolution and Ni deposition. In this study, the current density for H_2 evolution from the Zn–Ni alloy solution decreased once, despite a shift in the potential to the less noble direction in the region that was nobler than the equilibrium potential of Zn (Fig. 1(d)); this was attributed to suppression by $Zn(OH)_2$, formed through the multistep reactions of Zn deposition. The transition current densities at solution temperatures of 293 and 313 K were almost identical but they significantly increased at 333 K (Fig. 1(a)). Focusing on the effect of solution temperature on the partial current densities of Zn and Ni depositions and H_2 evolution in the transition current density region, it was found that the partial current densities of the H_2 evolution and Ni deposition were almost identical at solution temperatures of 293 and 313 K but clearly increased at 333 K (Figs. 1(b)–1(d)). That is, because the H_2 evolution and Ni deposition were promoted at 333 K, the current density that was required to complete Eqs. (1) and (2), *i.e.*, the transition current density, seems to increase with solution temperature.

In Zn–Ni alloy deposition, a competition reaction between the Zn and Ni depositions and H_2 evolution occurs. Hence, deposition was performed with solutions including only Ni or Zn to compare the effect of the solution temperature on each reaction. **Figure 6** shows the effect of solution temperature on the partial polarization curve for Ni deposition and H_2 evolution for the Ni solution. Both Ni deposition

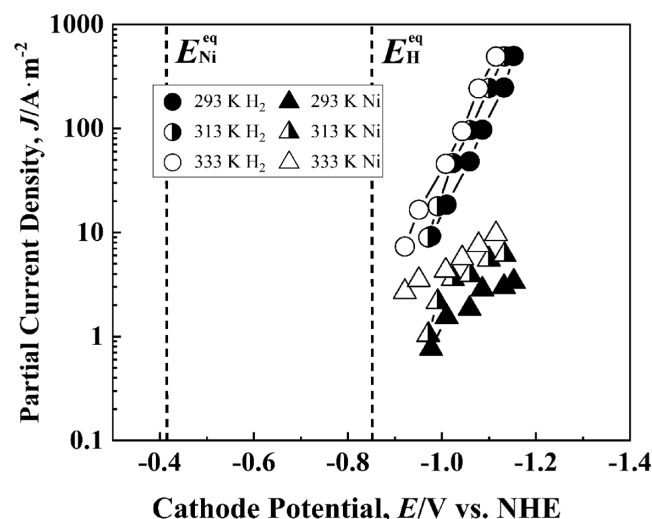


Fig. 6. Partial polarization curves for Ni deposition and H_2 evolution from the Ni only alkaline solutions at 293, 313 and 333 K.

and H_2 evolution were depolarized with increasing solution temperature. At a partial current density of $3 \text{ A} \cdot \text{m}^{-2}$ for Ni deposition, the potential shifted to the noble direction by approximately 0.2 V, when the solution temperature was raised from 293 to 333 K. At a partial current density of $100 \text{ A} \cdot \text{m}^{-2}$ for H_2 evolution, the potential shifted by approximately 0.06 V with increasing solution temperature, and the degree of depolarization was greater for Ni deposition. Here the overpotential for metal deposition, *i.e.*, η_M , is defined by the following equation:

$$\eta_M = |E_M^{\text{eq}} - E_M| \dots\dots\dots (6)$$

where E_M^{eq} is the equilibrium potential of metal deposition, and E_M is the electrode potential for metal deposition. Comparing the overpotential for Ni deposition with that for H_2 evolution, the one for Ni deposition was larger. **Figure 7** shows the effect of solution temperature on the current efficiency of Ni deposition from the Ni solution. The current efficiency for Ni deposition increased with increasing solution temperature at all current densities. Particularly, in the low-current-density region of $10\text{--}20 \text{ A} \cdot \text{m}^{-2}$, the current efficiency for Ni deposition significantly increased with solution temperature. Based on Figs. 6 and 7, it was found that both Ni deposition and H_2 evolution were promoted with increasing solution temperature, while an increase in solution temperature had a stronger promotional effect on the Ni deposition.

Figure 8 shows the effect of solution temperature on the partial polarization curve for Zn deposition from the Zn solution. The partial polarization curves for Zn deposition depolarized with increasing solution temperature. At 313 and 333 K, the Zn began to deposit near its equilibrium potential, indicating that the deposition overpotential was small. At a solution temperature of 293 K, the Zn deposition approached the diffusion limitation of Zn ions at approximately -1.6 V . **Figure 9** shows the effect of solution temperature on the current efficiency of Zn deposition from the Zn solution. In the low-current-density range of $10\text{--}20 \text{ A} \cdot \text{m}^{-2}$, the current efficiency for Zn deposition decreased with increasing solution temperature, indicating that an

increase in solution temperature had a stronger effect on H_2 evolution. Comparing the effects of solution temperature on the Zn and Ni depositions and H_2 evolution (Figs. 6–9), in the low-current density range, where the charge transfer process was rate-limiting, the degree of promotion with increasing solution temperature followed the order Ni deposition > H_2 evolution > Zn deposition. Zinc deposition from an aqueous solution is known to occur in the case where there is a small overpotential for deposition, whereas Ni deposition and H_2 evolution occur when there is a large overpotential for deposition since they proceed in the multistep reactions via adsorption intermediates NiOH_{ad} and H_{ad} , respectively and slow elementary process is present. As shown in Figs. 6 and 8, the overpotential for Zn deposition was small, even from the zincate solution, while that for Ni deposition was large. Since Ni deposition and H_2 evolution had an inherently large overpotential, the promotional effect of increasing the solution temperature on the Ni deposition and H_2 evolution appeared to have been stronger than that on the Zn deposition. In the deposition from the Ni solution, the promotional effect of increasing the solution

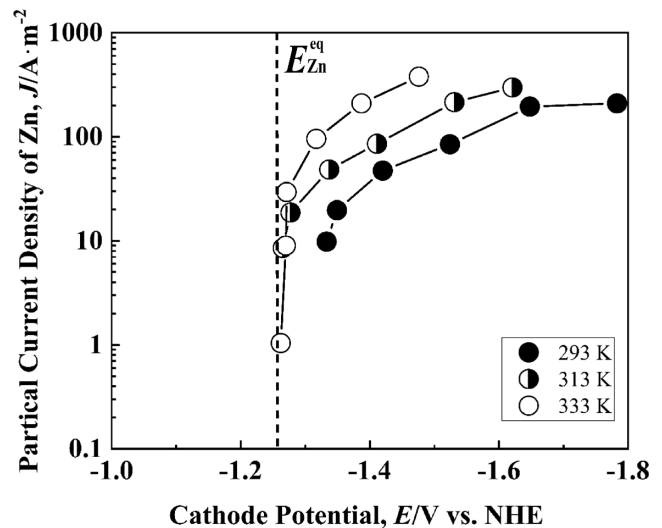


Fig. 8. Partial polarization curve for Zn deposition from Zn only alkaline solutions at 293, 313 and 333 K.

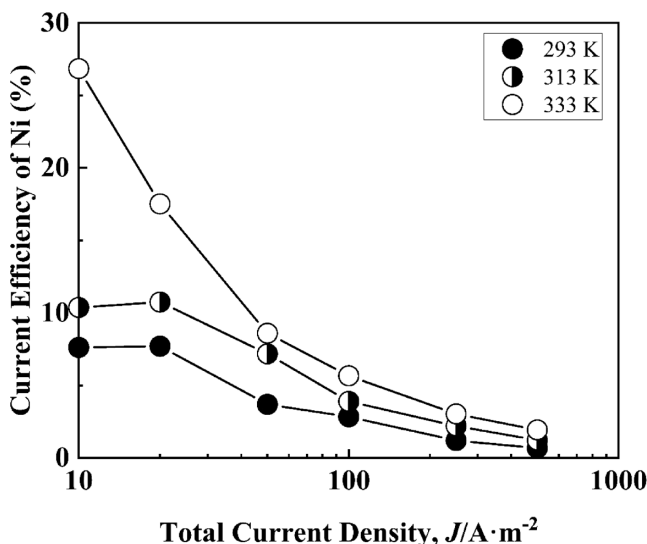


Fig. 7. Current efficiencies for Ni deposition from Ni only alkaline solutions at 293, 313 and 333 K.

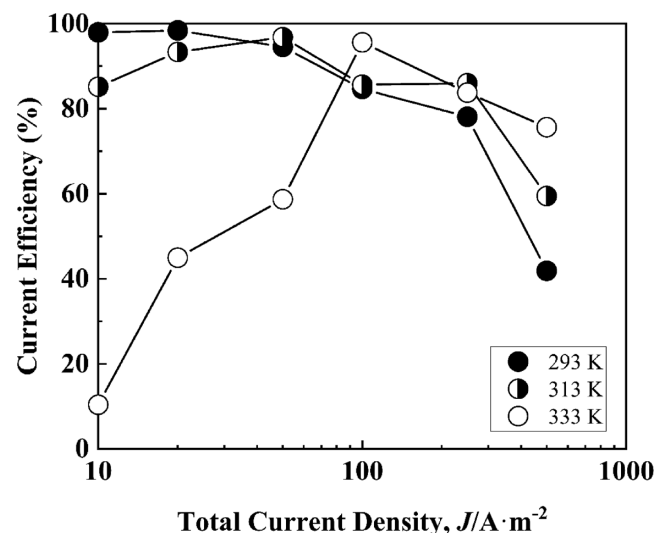


Fig. 9. Current efficiencies for Zn deposition from Zn only alkaline solutions at 293, 313 and 333 K.

temperature on the Ni deposition was larger than that on the H_2 evolution, which was attributed to the fact that the overpotential for Ni deposition was larger than that for H_2 evolution on Ni. Contrastingly, in the high-current density region of $500\text{ A}\cdot\text{m}^{-2}$, the current efficiency for Zn deposition increased with increasing solution temperature (Fig. 9). Since the diffusion of Zn ions became the rate-limiting step of the Zn deposition in the high-current density region, the current efficiency for Zn deposition seems to increase with increasing solution temperature due to the promotion of Zn ion diffusion.

The effect of solution temperature on the current efficiency for alloy deposition and the composition of the deposited films will be discussed next, based on the results for the solutions that included only Ni or Zn noted above. First, the current efficiency for alloy deposition increased with increasing solution temperature in both the normal ($10\text{--}50\text{ A}\cdot\text{m}^{-2}$) and anomalous ($500\text{ A}\cdot\text{m}^{-2}$) co-deposition regions (Fig. 2(a)). In the normal co-deposition region, the Ni content of the deposited films was approximately 90 mass%, revealing that the competition reaction between Ni deposition and H_2 evolution mainly occurred in this region. Ni deposition and H_2 evolution were both promoted with increasing solution temperature, but the promotional effect on the Ni deposition was stronger, as determined from the results for the Ni solution (Figs. 6 and 7). As a result, the current efficiency for alloy deposition increased with increasing solution temperature. In the normal co-deposition region of $10\text{--}50\text{ A}\cdot\text{m}^{-2}$, the current efficiency for alloy deposition decreased with increasing current density at all solution temperatures. This was attributed to increase in the formation rate of $Zn(OH)_2$ in the multistep reactions of Zn deposition, caused by increasing the current density and the suppression of Ni deposition by $Zn(OH)_2$. Contrastingly, in the anomalous co-deposition region at $500\text{ A}\cdot\text{m}^{-2}$, the Ni content in the deposited films was approximately 5 mass%, revealing that the competition reaction between Zn deposition and H_2 evolution occurred mainly in this region. The Zn deposition in this region appeared to proceed under a mixed rate-determining process that included the charge transfer and diffusion of Zn ions (Fig. 1(b)). The diffusion of Zn ions was promoted with increasing solution temperature, resulting in an increase in the current efficiency of the alloy deposition. Comparing the current efficiency of Ni deposition from the alloy solution and the single Ni solution, that from the alloy solution was observably higher (Figs. 2(c) and 7). This suggested that the formation of $Zn(OH)_2$ in the alloy solution suppressed both the H_2 evolution and Ni deposition but that the H_2 evolution was more strongly suppressed.

The Ni content in the deposited films increased with increasing solution temperature in both the normal ($10\text{--}50\text{ A}\cdot\text{m}^{-2}$) and anomalous ($250\text{--}500\text{ A}\cdot\text{m}^{-2}$) co-deposition regions (Fig. 3). The Zn and Ni depositions in the alloy deposition appeared to proceed under a rate-determining process comprising the charge transfer in the normal co-deposition region, while they appeared to follow a mixed rate-determining process comprising the charge transfer and diffusion of Zn^{2+} ions in the anomalous co-deposition region. Since Ni deposition was promoted to a greater degree than Zn deposition by increasing the solution tem-

perature in the region where the charge transfer process was rate-limiting, the Ni content in the deposited films seems to increase with solution temperature in both the normal and anomalous co-deposition regions.

As shown in Fig. 1(b), in the Zn–Ni alloy deposition, the Zn appeared to have been deposited in a potential region nobler than its equilibrium potential, whereas this phenomenon was not observed in the deposition from a single Zn solution (Fig. 8). It was reported that Zn–Ni alloy deposition in the potential range nobler than the equilibrium potential of Zn had been caused by the formation of a stable intermetallic compound, Ni_5Zn_{21} , through deposition, which considerably reduced the activity coefficient of the Zn in the deposited films.^{42–44} That is, the co-deposition of Ni is essential for the Zn apparently depositing in the potential region nobler than its equilibrium potential. In the present study, the deposition of Zn in the noble potential region is thought to be increased with temperature because the deposition of Ni was accelerated at a higher solution temperature.

Finally, we discuss the difference between the deposition behavior of the Zn–Ni alloy from the zincate solution in this study and that from a sulfate solution previously reported. The most important difference between the deposition from zincate and sulfate solutions was the cause of $Zn(OH)_2$ formation, which is an inhibitor of Ni deposition and H_2 evolution. In sulfate solutions, $Zn(OH)_2$ is formed by the hydrolysis of Zn^{2+} due to the increase of solution pH by the reduction of H^+ at the cathode. In contrast, in the zincate solution, it is thought to be formed in the intermediate stage of the multistep Zn deposition reactions. In the case of alloy deposition from sulfate solutions, it was reported that the Ni content in the deposited films was approximately 10 mass% in the region where an anomalous-type co-deposition occurred, which was much lower than the CRL (50 mass% Ni^{2+} content in the solution).²⁹ In the case of the present study, the Ni content in the deposited films from the zincate solution was approximately 5–8 mass% in the region where the anomalous co-deposition occurred (Fig. 3), which was below the CRL (8.7 mass%). However, the anomalies were greater in the sulfate solution than in the zincate solution (Fig. 3), indicating that the suppression of Ni deposition by $Zn(OH)_2$ was stronger. The difference in the degree of Ni deposition suppression between the sulfate and zincate solutions may have been due to difference in cause of $Zn(OH)_2$ formation. In the sulfate solution, the Ni content in the deposited films increased from approximately 10 mass% to approximately 25 mass% as the solution temperature increased from 303 to 333 K.³⁹ However, the increase in Ni content may be larger than that in the zincate solutions (Fig. 3) because the inhibitory effect of $Zn(OH)_2$ on the Ni deposition is stronger in the sulfate solution.

5. Conclusion

The effect of solution temperature on the deposition behavior of Zn–Ni alloys from alkaline zincate solutions was investigated. The transition current density at which the deposition behavior shifted from the normal to anomalous co-deposition was almost identical at solution temperatures of 293 and 313 K but clearly increased at 333 K. The transition current density appeared to increase due to the enhance-

ment of H₂ evolution and Ni deposition at 333 K. The current efficiency for alloy deposition also increased with increasing solution temperature in both the normal (10–50 A·m⁻²) and anomalous (500 A·m⁻²) co-deposition regions. In the normal co-deposition region, Ni deposition and H₂ evolution mainly occurred, and the promoting effect of increase in the solution temperature on the Ni deposition was greater than that on the H₂ evolution, resulting in an increase in current efficiency alongside solution temperature. In the anomalous co-deposition region at 500 A·m⁻², Zn deposition and H₂ evolution mainly occurred, and Zn deposition appeared to proceed under a mixed rate-determining process comprising the charge transfer and diffusion of Zn ions. Since the diffusion of Zn ions is promoted by increasing the solution temperature, the current efficiency also seems to increase. Furthermore, the Ni content in the deposited films increased with the solution temperature at all current densities. In the region where the charge transfer process is rate-limiting, Ni deposition accelerates to a greater degree compared with Zn deposition alongside increasing solution temperature, as a result, Ni content in the deposited films seems to increase. In addition, the γ -phase of the deposited films increased with increasing solution temperature.

Acknowledgement

This work was supported by JST SPRING, Grant Number JPMJSP2136.

REFERENCES

- 1) S. Ghaziof and W. Gao: *Appl. Surf. Sci.*, **311** (2014), 635. <https://doi.org/10.1016/j.apsusc.2014.05.127>
- 2) S. H. Mosavat, M. H. Shariat and M. E. Bahrololoom: *Corros. Sci.*, **59** (2012), 81. <https://doi.org/10.1016/j.corsci.2012.02.012>
- 3) R. M. Gnanamuthu, S. Mohan, G. Saravanan and C. W. Lee: *J. Alloy. Compd.*, **513** (2012), 449. <https://doi.org/10.1016/j.jallcom.2011.10.078>
- 4) M. Tafreshi, S. R. Allahkaram and H. Farhangi: *Mater. Chem. Phys.*, **183** (2016), 263. <https://doi.org/10.1016/j.matchemphys.2016.08.026>
- 5) K. Wykpiś, M. Popczyk, J. Niedbała, A. Budniok and E. Łagiewka: *Mater. Sci.*, **47** (2012), 838. <https://doi.org/10.1007/s11003-012-9463-4>
- 6) T. V. Gaevskaya, T. V. Byk and L. S. Tsybul'skaya: *Russ. J. Appl. Chem.*, **76** (2003), 1583. <https://doi.org/10.1023/B:RJAC.0000015717.21845.5e>
- 7) Z. Feng, Q. Li, J. Zhang, P. Yang, H. Song and M. An: *Surf. Coat. Technol.*, **270** (2015), 47. <https://doi.org/10.1016/j.surfcoat.2015.03.020>
- 8) J. Panek, B. Bierska-Piech, E. Łagiewka and A. Budniok: *Surf. Interface Anal.*, **42** (2010), 1226. <https://doi.org/10.1002/sia.3205>
- 9) H. Fukushima, T. Akiyama, J.-h. Lee, M. Yamaguchi and K. Higashi: *J. Met. Finish. Soc. Jpn.*, **33** (1982), 574 (in Japanese). <https://doi.org/10.4139/sfj1950.33.574>
- 10) H. Fukushima, T. Akiyama, M. Yano, T. Ishikawa and R. Kammel: *ISIJ Int.*, **33** (1993), 1009. <https://doi.org/10.2355/isijinternational.33.1009>
- 11) H. Nakano, S. Kobayashi, T. Akiyama, T. Tsuru and H. Fukushima: *Tetsu-to-Hagane*, **89** (2003), 64 (in Japanese). https://doi.org/10.2355/tetsutohagane1955.89.1_64
- 12) H. Nakano, M. Matsuno, S. Oue, M. Yano, S. Kobayashi and H. Fukushima: *J. Jpn. Inst. Met.*, **69** (2005), 548 (in Japanese). <https://doi.org/10.2320/jinstmet.69.548>
- 13) A. El Hajjami, M. P. Gigandet, M. De Petris-Wery, J. C. Catonne, J. J. Duprat, L. Thiery, F. Raulin, N. Pommier, B. Starck and P. Remy: *Appl. Surf. Sci.*, **254** (2007), 480. <https://doi.org/10.1016/j.apsusc.2007.06.016>
- 14) A. Conde, M. A. Arenas and J. J. de Damborenea: *Corros. Sci.*, **53** (2011), 1489. <https://doi.org/10.1016/j.corsci.2011.01.021>
- 15) H. Nakano, M. Matsuno, S. Oue, M. Yano, S. Kobayashi and H. Fukushima: *Mater. Trans.*, **45** (2004), 3130. <https://doi.org/10.2320/matertrans.45.3130>
- 16) G. W. Loar, K. R. Romer and T. J. Aoe: *Plat. Surf. Finish.*, **78** (1991), 74.
- 17) G. Y. Li, J. S. Lian, L. Y. Niu and Z. H. Jiang: *Surf. Coat. Technol.*, **191** (2005), 59. <https://doi.org/10.1016/j.surfcoat.2004.04.062>
- 18) C. Müller, M. Sarret and M. Benbaila: *J. Electroanal. Chem.*, **519** (2002), 85. [https://doi.org/10.1016/S0022-0728\(01\)00725-2](https://doi.org/10.1016/S0022-0728(01)00725-2)
- 19) H. Y. Lee and S. G. Kim: *Surf. Coat. Technol.*, **135** (2000), 69. [https://doi.org/10.1016/S0257-8972\(00\)00731-3](https://doi.org/10.1016/S0257-8972(00)00731-3)
- 20) R. Pfiz and G. Strube: *Trans. IMF*, **74** (1996), 158. <https://www.tandfonline.com/doi/abs/10.1080/00202967.1996.11871117>
- 21) L. S. Tsybul'skaya, T. V. Gaevskaya, O. G. Purovskaya and T. V. Byk: *Surf. Coat. Technol.*, **203** (2008), 234. <https://doi.org/10.1016/j.surfcoat.2008.08.067>
- 22) H. Nakano, S. Arakawa, S. Oue and S. Kobayashi: *ISIJ Int.*, **53** (2013), 1864. <https://doi.org/10.2355/isijinternational.53.1864>
- 23) S. Haruyama: Hyomen Gijutsusha no tameno Denkikagaku (Electrochemistry for Surface Engineer), Maruzen, Tokyo, (2005), 173 (in Japanese).
- 24) M. Pourbaix: Atlas of Electrochemical Equilibria in Aqueous Solutions, Pergamon Press, Oxford, UK, (1966), 406.
- 25) D. D. Perrin: Stability Constants of Metal-ion Complexes, Part B, Organic Ligands, Pergamon Press, Oxford, UK, (1979), 466.
- 26) T. Akiyama, H. Fukushima and K. Higashi: *Tetsu-to-Hagane*, **72** (1986), 918 (in Japanese). https://doi.org/10.2355/tetsutohagane1955.72.8_918
- 27) S. H. Bae, S. Oue, I. Son and H. Nakano: *ISIJ Int.*, **61** (2021), 2256. <https://doi.org/10.2355/isijinternational.ISIJINT-2021-080>
- 28) S. H. Bae, S. Oue, I. Son and H. Nakano: *Tetsu-to-Hagane*, **107** (2021), 229 (in Japanese). <https://doi.org/10.2355/tetsutohagane.TETSU-2020-108>
- 29) T. Akiyama and H. Fukushima: *Shigen-to-Sozai*, **112** (1996), 583 (in Japanese). <https://doi.org/10.2473/shigentosozai.112.583>
- 30) H. Nakano, S. Oue, D. Yoshihara, H. Fukushima, Y. Saka, S. Sawada and Y. Hattori: *Mater. Trans.*, **52** (2011), 1237. <https://doi.org/10.2320/matertrans.M2011022>
- 31) H. Nakano, S. Oue, D. Yoshihara, H. Fukushima, Y. Saka, S. Sawada and Y. Hattori: *J. Jpn. Inst. Met.*, **75** (2011), 61 (in Japanese). <https://doi.org/10.2320/jinstmet.75.61>
- 32) H. Fukushima and H. Nakano: *J. Surf. Sci. Soc. Jpn.*, **22** (2001), 107 (in Japanese). <https://doi.org/10.1380/jssj.22.107>
- 33) H. Nakano, T. Ohgai, H. Fukushima, T. Akiyama and R. Kammel: *Metall.*, **55** (2001), 676.
- 34) H. Fukushima, T. Akiyama and K. Kiyotani: *Shigen-to-Sozai*, **109** (1993), 861 (in Japanese). <https://doi.org/10.2473/shigentosozai.109.861>
- 35) T. Yamashita and S. Toshima: *Nippon Kagaku Kaishi*, **1980** (1980), 1824 (in Japanese). <https://doi.org/10.1246/nikkashi.1980.1824>
- 36) K. Aotani: Gokin Mekki VI (Alloy Plating VI), Nippon Plating Kyokai, Tokyo, (2005), 133 (in Japanese).
- 37) T. Yoshida: Saishin Hyomen Shori Gijutsu Soran (New Engineering Review of Coating), Sangyo Gijutsu Service Center, Tokyo, (1987), 318 (in Japanese).
- 38) K. Fukuda, Y. Kashiwa, S. Oue, T. Takasu and H. Nakano: *ISIJ Int.*, **61** (2021), 919. <https://doi.org/10.2355/isijinternational.ISIJINT-2020-105>
- 39) K. Fukuda, Y. Kashiwa, S. Oue, T. Takasu and H. Nakano: *Tetsu-to-Hagane*, **105** (2019), 988 (in Japanese). <https://doi.org/10.2355/tetsutohagane.TETSU-2019-045>
- 40) K. Fukuda, Y. Kashiwa, S. Oue, T. Takasu and H. Nakano: *ISIJ Int.*, **59** (2019), 1632. <https://doi.org/10.2355/isijinternational.ISIJINT-2019-023>
- 41) Y. Kashiwa, N. Nagano, T. Takasu, S. Kobayashi, K. Fukuda and H. Nakano: *ISIJ Int.*, **59** (2019), 514. <https://doi.org/10.2355/isijinternational.ISIJINT-2018-676>
- 42) H. Nakano, S. Arakawa, Y. Takada, S. Oue and S. Kobayashi: *J. Jpn. Inst. Met.*, **76** (2012), 443 (in Japanese). <https://doi.org/10.2320/jinstmet.76.443>
- 43) H. Nakano, S. Arakawa, S. Oue and S. Kobayashi: *Tetsu-to-Hagane*, **99** (2013), 425 (in Japanese). <https://doi.org/10.2355/tetsutohagane.99.425>
- 44) H. Nakano, S. Arakawa, Y. Takada, S. Oue and S. Kobayashi: *Mater. Trans.*, **53** (2012), 1946. <https://doi.org/10.2320/matertrans.M2012241>